Nat Med. Author manuscript; available in PMC 2014 May 01.

Published in final edited form as:
Nat Med. 2013 November ; 19(11): 1524–1528. doi:10.1038/nm.3356.

Chloride extrusion enhancers as novel therapeutics for neurological diseases

Martin Gagnon[1,2,3,*], **Marc J. Bergeron**[1,2,*], **Guillaume Lavertu**[1,2], **Annie Castonguay**[1,2], **Sasmita Tripathy**[3], **Robert P. Bonin**[1,2], **Jimena Perez-Sanchez**[1,2], **Dominic Boudreau**[1,2], **Bin Wang**[3], **Lionel Dumas**[3], **Isabelle Valade**[3], **Karine Bachand**[1,2], **Mariève Jacob-Wagner**[5], **Christian Tardif**[1,4], **Irenej Kianicka**[3], **Paul Isenring**[5], **Giorgio Attardo**[3], **Jeffrey A.M. Coull**[3], and **Yves De Koninck**[1,2,4]

[1]Institut universitaire en santé mentale de Québec, Qc

[2]Department of Psychiatry & Neuroscience, Université Laval, Québec, Qc

[3]Chlorion Pharma, Inc. Laval, Qc

[4]Graduate program in biophotonics, Université Laval, Québec, Qc

[5]Centre de recherche du Centre Hospitalier Universitaire de Québec, Qc

Abstract

The K^+-Cl^- cotransporter KCC2 is responsible for maintaining low Cl^- concentration in neurons of the central nervous system (CNS), essential for postsynaptic inhibition through $GABA_A$ and glycine receptors. While no CNS disorders have been associated with KCC2 mutations, loss of activity of this transporter has emerged as a key mechanism underlying several neurological and psychiatric disorders including epilepsy, motor spasticity, stress, anxiety, schizophrenia, morphine-induced hyperalgesia and chronic pain[1–9]. Recent reports indicate that enhancing KCC2 activity may be the favoured therapeutic strategy to restore inhibition and normal function in pathological condition involving impaired Cl^- transport[10–12]. We designed an assay for high-throughput screening which led to the identification of KCC2 activators that reduce $[Cl^-]_i$. Optimization of a first-in-class arylmethylidine family of compounds resulted in a KCC2-selective analog (CLP257) that lowers $[Cl^-]_i$. CLP257 restored impaired Cl^- transport in neurons with diminished KCC2 activity. The compound rescued KCC2 plasma membrane expression, renormalised stimulus-evoked responses in spinal nociceptive pathways sensitized after nerve injury and alleviated hypersensitivity in a rat model of neuropathic pain. Oral efficacy for analgesia equivalent to that of

Please send correspondence to: Yves De Koninck, Division of Cellular and Molecular Neuroscience, Institut universitaire de santé mentale de Québec, 2601, Chemin de la Canardière, Québec, QC, G1J 2G3, CANADA, Phone: 418-663-5747 ext. 6885, FAX: 418-948-9030, Yves.DeKoninck@crulrg.ulaval.ca.
*These authors contributed equally in this work.

AUTHOR CONTRIBUTIONS

M.G., J.A.M.C., and Y.D.K. conceived and designed the project. M.G., J.A.M.C., P.I., I.K. and Y.D.K. supervised the experiments. M.G., M.J.B., G.L., A.C.,, R.P.B., J.P.-S., D.B., K.B and M.J.W. performed the experiments. G.A., S.T., B.W., L.D., I.V. designed and synthesized analogs of CL-058. M.G., M.J.B., G.L., A.C., R.P.B., J.P.-S., D.B., M.J.-W., C.T. and I.K. analyzed the data. M.G., M.J.B., G.L., A.C., R.P.B. and Y.D.K. wrote the manuscript. All of the authors read and discussed the manuscript.

Pregabalin but without motor impairment was achievable with a CLP257 prodrug. These results validate KCC2 as a druggable target for CNS diseases.

Keywords

Neuropathic pain; K^+-Cl^- cotransporter 2; KCC2; Cl^- homeostasis; disinhibition; novel analgesics; drug discovery

To identify compounds that increase Cl^- efflux, a simple fluorometric assay was developed to measure $[Cl^-]_i$ in real-time. As a model, we chose the NG-108 cell line which expresses low levels of KCC2 protein (Fig. 1a), and in which the Cl^--sensitive indicator clomeleon[13] was stably transfected. The low KCC2 activity of NG-108 cells mimics the pathophysiological situation in neuropathic pain. The fluorometric assay was calibrated and validated by placing NG108-cl and KCC2-lacking HEK293-cl cells[14–16] in isosmolar extracellular media containing increasing $[Cl^-]$ in permeabilized cells to clamp $[Cl^-]_i$ at different levels. We found a linear relationship between the fluorescence ratio and $[Cl^-]_i$ in both cell lines and determined a resting $[Cl^-]_i$ of 57.15 ± 2.43 mM (SD) for NG108-cl and 56.15 ± 2.73 mM (SD) for HEK293-cl (Fig. 1b). In non-permeabilized NG108-cl cells $[Cl^-]_i$ did not change with increasing $[Cl^-]_e$, indicating little endogenous Cl^- transport in these cells (Fig. 1a). In contrast, $[Cl^-]_i$ varied slightly in HEK293-cl when $[Cl^-]_e$ was elevated, consistent with their higher NKCC1 expression (Fig. 1a). The fluorescence ratio within the range of $[Cl^-]_i$ tested was minimally affected by pH (Fig. 1b). High-throughput screening of a 92,500 drug-like[17] compound library was then carried out to identify small molecules able to reduce $[Cl^-]_i$. A total of 78 were confirmed as positive hits. Many of these compounds could be grouped into chemical families sharing similar structure. Hits were further selected for lack of effects on $[Cl^-]_i$ in HEK293-cl cells, which do not express KCC2 but do express NKCC1, KCC1, KCC3 and KCC4[16,18] (Fig. 1a). Further selection based on lack of cytotoxic effects, ease of synthesis and drug-like properties[17] identified the hit compound CL-058 for further characterization and optimization (Fig. 1c,d).

More than 300 unique analogues of CL-058 were synthesized to improve potency and drug-like properties[17]. This lead optimization campaign defined a clear structure-activity relationship (Supplementary Fig. 1; Supplementary Table 1), and improved on the potency of CL-058 (EC_{50} = 31.5 μM) by almost 3 logs with compounds such as CLP355 (EC_{50} = 50 nM; Fig. 1d). CLP257 (EC_{50} = 616 nM) was chosen for further characterization due to its better chemical stability and overall properties. Maximal $[Cl^-]_i$ reduction by CLP257 was ~40%, a 23mM drop from resting $[Cl^-]_i$ of 57 mM.

We found no change in $[Cl^-]_i$ in HEK293-cl cells when incubated with CLP257 (Fig. 1e), indicating inactivity on NKCC1, KCC1, KCC3 or KCC4. Additionally, a Rb^+-flux assay of CLP257 selectivity was performed in *Xenopus laevis* oocytes microinjected with cRNA coding for the various transporters of the cation chloride cotransporter (CCC) family (Fig. 1f). Oocyte pre-incubation with CLP257 (200 nM) increased KCC2 transport activity by 61% ($P < 0.01$), but caused no change in other CCCs (Fig. 1f). Functional, dose-dependent antagonism was also observed between CLP257 and the recently characterized KCC2 antagonist VU0240551[19] (Fig. 1g). The affinity of CLP257 for classical pharmacological

targets was also assessed using radioligand competition binding assays. Of the 55 radioligand-receptor interactions tested, none were inhibited by more than 30% at 10 μM of CLP257 (Supplementary Table 2). Importantly, CLP257 (50 μM) provoked < 0.2% of the effect of 5 μM muscimol in CHO cells transduced with recombinant α1β2γ2 $GABA_A$ receptors, indicating negligible agonist activity of CLP257 on $GABA_A$. receptors. Taken together these data show that CLP257 reduces $[Cl^-]_i$ through selective modulation of KCC2.

We then tested whether CLP257 could reverse KCC2 hypofunction in mature neurons. The effect of CLP257 on Cl^- transport was measured in spinal slices obtained from animals with peripheral nerve injury (PNI; as an experimental model of neuropathic pain)[20] and control slices pre-treated with brain-derived neurotrophic factor (BDNF), which mediates downregulation of KCC2 activity[21,22] in models of pain hypersensitivity[3,9,23–27]. The function of KCC2 was assessed by quantitatively measuring K^+-driven Cl^- influx via fluorescent lifetime measurements of the Cl^- probe MQAE[10] (Fig. 2a,b,c). Using abrupt elevation of $[K^+]_e$ to trigger KCC2-dependent Cl^- influx, we found that CLP257 (25 μM) significantly increased the rate of Cl^- accumulation in both BDNF-treated and PNI spinal slices by 26% and 45%, respectively (Fig. 2d,e; $P < 0.05$). At 100 μM, CLP257 completely restored Cl^- transport to control levels in BDNF-treated slices. Thus, CLP257effectively enhanced Cl^- transport in CNS neurons with reduced KCC2 function.

We tested whether CLP257 modulates Cl^- extrusion capacity using voltage-clamp recordings from superficial dorsal horn (SDH) neurons in spinal cord slices treated with BDNF and isolated from rats with PNI[3]. A Cl^- load was imposed through the recording pipette to measure Cl^- extrusion capacity via the reversal potential for $GABA_A$ currents (E_{GABA})[9]. E_{GABA} was depolarized in SDH neurons of BDNF-treated and PNI slices (Fig. 2f,g,h). In both conditions, E_{GABA} was hyperpolarized by 25 μM CLP257 (Fig. 2h), reflecting an increase in neuronal Cl^- extrusion capacity. Thus, CLP257 can restore Cl^- extrusion capacity in neurons with reduced KCC2 activity[23]. The effects of CLP257 on E_{GABA} were independent of changes in $GABA_A$ conductance, since acute application of CLP257 had no effect on evoked $GABA_A$ currents in the presence of the KCC2 antagonist VU0240551 ($P > 0.05$; Fig. 2i).

To identify the mechanism by which CLP257 restored KCC2 activity, we immunoblotted KCC2 protein in BDNF-pretreated slices. We found that, while total KCC2 expression was not significantly affected ($P > 0.05$), the cell surface expression of both KCC2 monomers and dimers was increased in CLP257-treated slices (Fig. 3a,b; $P < 0.05$). This indicates that CLP257 modulates plasmalemmal KCC2 protein turnover post-translationally.

The antinociceptive efficacy of CLP257 was tested in PNI rats[3,20,28,29] (Fig. 4a–d). We measured evoked field electrophysiological responses in the superficial dorsal horn to graded mechanical stimuli of the hind foot. In naïve animals, CLP257 had no effect on the stimulus-response relationship over the entire range of stimulus intensity (2.5 to 135 g $(mm^2)^{-1}$; Fig. 4a,c,d). Evoked field responses were increased in animals with nerve injury (Fig. 4d; $P < 0.05$), but were renormalized by CLP257 (Fig 4b,c,d.).

CLP257 also normalized mechanical withdrawal thresholds in PNI animals. Intraperitoneal (IP) administration of CLP257 increased withdrawal thresholds, peaking at 100 mg kg^{-1}, 2 h post-injection (Fig. 4e). Yet, the maximal analgesic effect of CLP257 was much weaker than that of Gabapentin (Fig. 4e). We hypothesized that a poor pharmacokinetic profile could limit CLP257 efficacy. Indeed, pharmacokinetic analysis revealed that plasma concentration of CLP257 declines rapidly, with a terminal half-life ($t_{1/2}$) of < 15 min (Fig. 4f). Metabolite analyses revealed that the hydroxyl moiety of CLP257 rapidly undergoes glucuronidation (not shown) to produce an inactive metabolite (see CLP386, Supplementary Table 1)

To improve the pharmacokinetics of CLP257, a carbamate prodrug (CLP290) was designed to protect the hydroxyl group from glucuronidation. The pharmacokinetic profile of CLP257 produced from the metabolism of CLP290 was much improved over that of native CLP257, with an apparent $t_{1/2}$ of 5 h and improved maximal plasma concentration and exposure (Fig. 4f). The analgesic efficacy of CLP290 was also improved, with maximal oral efficacy equivalent to that of Pregabalin albeit at a higher dose (100 mg kg^{-1} vs 30 mg kg^{-1}; Fig. 4g).

Pregabalin can cause sedation and dizziness, greatly affecting motor performance[30]. For comparison, the motor impact of equipotent oral doses of CLP290 and Pregabalin was evaluated using an accelerating rotorod. While Pregabalin depressed motor function, CLP290 had no effect (Fig. 4h). These results show that modulating $[Cl^-]_i$ produces analgesia without motor side effects often seen with other analgesics.

To assess toxicity of CLP290, a 7-day repeat-dose study in rats was performed, with a maximum daily dose of 2000 mg kg^{-1}. We observed no effect of CLP290 on clinical condition, body weight, food consumption, hematology, coagulation, clinical chemistry, urinalysis, organ weight, pathology and histopathology (Supplementary Table 3). The inhibition of hERG tail current, a common risk factor for cardiotoxicity, by CLP257 and CLP290 was weak and therefore of low risk (IC_{50} 449 μM and 224 μM, respectively). Caspase-3 activation, a key process in apoptosis, was also not detected in rat hepatoma H4IIE cells *in vitro* after 24-h exposure to CLP257 at up to 300 μM.

This work validates KCC2 as a druggable target and Cl^- modulation as a novel mechanism of action for the development of therapeutics[31]. The expression of KCC2 is limited to the central nervous system, unlike other CCCs that are expressed in several tissues[3,12,32,33,34] such as the kidneys and blood vessels where ionic homeostasis is important. This constrained expression makes KCC2 a prime target for the control of neuronal $[Cl^-]_i$ and should limit adverse side-effects in other organs (*e.g.*, not expressed in choroid plexus, inner ear or sensory fibers[3,12,32,33]). In fact, unlike other KCCs (KCC1, KCC3 and/or KCC4), KCC2 is not involved in volume regulation and typically not found in cells where these KCCs are expressed[12].

The identification of a mechanism underlying neuropathic pain has allowed the development of this new class of compounds directly aimed at hypersensitivity. Drug development was previously limited by the poor understanding of the pathophysiology of neuropathic pain[35] as reflected by the classes of currently approved drugs such as anticonvulsants[36], antidepressants[37] and opioid narcotics[38]. As evidence is mounting that KCC2 dysfunction

and Cl^- homeostasis are central to many CNS disorders[1–8], we believe that Cl^- extrusion enhancers such as CLP257 and CLP290 represent a novel and important new method of treatment for a wide range of neurological and psychiatric indications.

Materials and Methods

All experimental procedures were performed in accordance with guidelines from the Canadian Council on Animal Care.

Cell culture, transfection, and lysis

Human embryonic kidney 293 (HEK293) and neuroblastoma/glioma-derivative NG108-15 (NG108) cells were grown on non-coated 10 cm plates, and maintained in DMEM/High Glucose medium (Thermo Scientific) supplemented with 10% fetal bovine serum and 50 U ml^{-1} penicillin/streptomycin mixtures (Invitrogen), with the addition of 100 μM hypoxanthine, 0.4 μM aminopterin, 16 μM thymidine (1x HAT) to NG108 cells. Cell lines were stably transfected with pcDNA3.1-Clomeleon using Escort IV reagent (Sigma) and kept under selection with G418 (Sigma, 200 μg ml^{-1} for HEK293-cl and 400 μg ml^{-1} for NG108-cl). Cells were propagated at 37 °C in a humidified atmosphere of 95% air and 5% CO_2. Rat hippocampal cultures were prepared as described previously[39]. Rat hippocampi were dissected out from post-natal day 0 rats and cells were dissociated, grown on poly-d-lysine coated 3,5cm plates (1×10^6 cells), and maintained for 5 days in Neurobasal medium supplemented with B27 (50:1), 50 U/ml penicillin/streptomycin mixtures, and 0.5 mM L-glutamax, and for 5 additional days with 5 μM of cytosine arabinofuranoside (ARA-C; Sigma)to reduce the number of glial cells. Afterwards, neurons were maintained in growth medium and propagated at 37°C in a humidified atmosphere of 95% air and 5% CO_2 and lysed at 20 DIV. Cells were lysed at ~ 80–90% confluence in 1 ml RIPA buffer (50 mM Tris-HCl pH 7.4, 150 mM NaCl, 1% Triton X-100, 0.5% Na-deoxycholate, and 0.1% SDS) supplemented with Complete® protease inhibitor cocktail (Roche). After incubation on a rotator (overnight; 4°C) and centrifugation at 18,000 g (15 min; 4 °C), supernatants were transferred into new tubes and labelled total cell lysates. Total protein concentration was determined using the Bio-Rad DC™ Protein Assay.

Immunoprecipitation studies

After incubation of ~1 mg total proteins with 5 μl of monoclonal mouse anti-KCC2 (clone N1/12) antibodies (Neuromab) on a rotator (overnight; 4°C), KCC2 protein was purified by addition of 50 μl RIPA-solubilised Protein A Sepharose™ CL-4B (GE Healthcare; overnight; 4°C), and recovery of the beads by centrifugation at 9,000 g (1 min; 4°C). Finally, immunoprecipitated KCC2 protein was released from the beads by boiling in 50μl 2x protein sample buffer, and subjected to SDS-PAGE and Western analyses.

Cell surface biotinylation

Two rat horizontal spinal dorsal horn slices (300 μm-thick) were kept alive during 5 h in bubbled ACSF at 34 °C. After 1h recovery, slices were treated for 2 h with 50 ng/ml BDNF, cut longitudinally (the two same lateral sides were subjected to the same treatment) and treated for an additional 2h with BDNF + DMSO or 100 μM CLP257. Treatment was ended

by washing slices twice in ice-cold 1X PBS. Slices were incubated (1 h; 4 °C) with 1.5 mg/ml EZ-Link® Sulfo-NHS-LC-Biotin (Thermo Scientific) in ice-cold 1X PBS buffer, washed with ice-cold quenching solution (100 mM glycine in 1X PBS) and lysed (0,5 ml RIPA buffer + Complete®) as described above. Biotinylated cell surface proteins were purified from ~300 μg total lysate proteins by adding 50 μl of slurry streptavidin agarose beads (Thermo Scientific; overnight; 4°C), and recovering the beads by centrifugation at 9,000 g (1 min; 4 °C). Finally, biotinylated cell surface proteins were released from the beads by boiling in 40 μl of 2x protein sample buffer, and subjected to SDS-PAGE and Western blot analyses. Validation of biotinylation assay in live slices is shown by the absence of any immunoreactive signal of the intracellular structural protein β-actin (Fig. 3a).

SDS-PAGE and Western blot analyses

Total proteins (5–10 μg), cell surface biotinylated-proteins (15 μl), and immunoprecipitated-KCC2 proteins (15 μl) were run on 8% Tris-Tricine SDS/polyacrylamide gels or on Any kD™ TGX gels (Bio-Rad). Gels were transferred onto Immobilon-P membrane blots (Bio-Rad) for Western blot analyses. Blots were sequentially incubated with primary and secondary antibodies. The primary antibodies, polyclonal rabbit anti-KCC2 (Upstate), mouse monoclonal anti-NKCC1 (Developmental Studies Hybridoma Bank) and anti-β-actin (Sigma), were used at a dilution of 1/1,000, 1/500 and 1/40,000, respectively. The secondary antibodies, streptavidin-HRP (Cell Signalling Technology), and goat anti-rabbit IgG-HRP-conjugated (Promega) and anti-mouse IgG (H+L)-HRP conjugate (Bio-Rad), were used at a dilution of 1/2,000, 1/15,000 and 1/5,000 respectively.

Normalization of KCC2 expression

The intensity of each band on immunoblots was measured using ImageJ (NIH). Cell surface expression of KCC2 was evaluated by the ratio cell surface expression/total expression (surface/total). This ratio was calculated by normalizing first the KCC2 cell surface expression to total biotinylated cell surface proteins (using streptavidin-HRP antibodies) and the KCC2 total expression to total proteins (using anti-β-actin antibodies), and normalized a second time, by dividing the normalized KCC2 cell surface expression by the normalized KCC2 total expression.

Clomeleon assay

NG108-cl or HEK293-cl (~2×10^6) cells were grown in 96-well plates in a low Cl^- assay medium (in mM: 30 HEPES, 2 $CaCl_2$, 2 $MgSO_4$, 10 K gluconate, 2 NaH_2PO_4, adjusted to pH 7.4 and 310 mOsm with Na gluconate). Validation of the assay was performed by adding an equal volume of assay media at pH 7.4 and containing varying [Cl^-] or varying pH and containing 100 mM NaCl, with or without 0.15% Triton X-100. Test articles (CLP257 and other compounds or DMSO vehicle, 4 replicates per condition) were prepared in high Cl^- assay media (in mM: 30 HEPES, 2 $CaCl_2$, 2 $MgSO_4$, 10 K gluconate, 2 NaH_2PO_4, 100 NaCl, adjusted to 310 mOsm with Na gluconate) and added to the cells in an equal volume, resulting in a final $[Cl^-]_e$ of 50 mM. Low Cl^- assay media containing 0.15% Triton X-100) was used as positive control. $[Cl^-]_i$ was measured using a fluorescence microplate reader (PerkinElmer Fusion, Ex 415 nm, Em 485 nm and 535 nm). Results are expressed as percent $[Cl^-]_i$ reduction after standardizing untreated cells to 0% $[Cl^-]_i$ reduction and cells treated

with low Cl^-/0.15% Triton X-100 assay media to 100% $[Cl^-]_i$ reduction. High-throughput screening was conducted by scaling down the assay to 384-well plates and testing a 92,500 compound library (Chemdiv, Panlabs) at 10 μM in single replicates using conditions as above. Compounds showing $[Cl^-]_i$ reduction greater than 3 standard deviations from negative control were retested in triplicate to confirm activity.

Rb^+ flux assays

Defolliculated stage V–VI Xenopus laevis oocytes were microinjected with 10 ng of cRNA coding for the various CCCs, and maintained for 3 days at 18°C in Barth's medium plus 125 μM furosemide. Oocytes were pre-incubated for 1h in a hypotonic solution (~55 mM Cl^- and 125 mOsm) for KCC1, KCC3 and KCC4, a low Cl^-/hypertonic solution (~5 mM Cl^- and 285mOsm) for NKCC1 and NKCC2, and a physiological solution (86mM Cl^- and ~200mOsm) for KCC2, containing either CLP257 or DMSO. Unlike KCC2 that functions in isotonic conditions, KCC1, KCC3 and KCC4 require a cell swelling stimulus to be activated. Oocytes were then incubated for another 45 min in a regular flux medium containing either CLP257 or DMSO, bathed several times in a wash solution and lysed in pure nitric acid[16]. Rb^+ content was measured by atomic absorption spectrometry (Varian AA240). All steps were carried out at room temperature. Results are expressed as percent change of Rb^+ influx in compound-treated oocytes versus Rb^+ influx in vehicle-treated oocytes.

Imaging of Cl^- transport in rat spinal neurons

Parasagittal spinal slices (400 μm-thick) were kept alive prior to imaging during ~5.5 h in bubbled ACSF at 34 °C. For PNI rats, imaging was performed on slices ipsilateral to the nerve injury. For naïve rats, after 1 h recovery, slices were treated for 2 h with 50 ng ml^{-1} BDNF and for an additional 2 h with BDNF and DMSO or different CLP257 concentrations. Slices were then incubated in ACSF containing 5 mM of the Cl^- indicator MQAE (N-6-methoxyquinolinium acetoethylester, Molecular Probes) for 30–40 min and transferred to a perfusion chamber (2 ml min^{-1}). Extracellular MQAE was washed out for 10 min in the presence of 1 μM tetrodotoxin, 10 μM CNQX, 40 μM AP5, 1 μM strychnine and 10 μM gabazine to minimize KCC2-independent Cl^- transport. Fluorescence lifetime imaging of MQAE was conducted as previously described[9,10]. Instrument response function of the detection path was acquired using an 80-nm gold nanoparticle suspension to generate second-harmonic signal. Recorded cells were visually identified by merging transmitted light and MQAE fluorescence. Lifetime images were acquired every 10 s for a period of 7 min. After a control period of 50 s, perfusion solution was switched to ACSF containing 15 mM KCl (osmolarity adjusted using mannitol) to reverse KCC2-mediated Cl^- transport[40]. Lifetime in each cell was averaged over the whole cell body area and extracted for each time point using custom-made Matlab software. Lifetime changes for each slice were then expressed as the mean of changes occurring in each cell. Briefly, based on the work of Digman et al.[41], we converted the photon timing histograms of each acquired lifetime image to phasor plots. Then, for every time-point, regions of interest (ROIs) corresponding to cell bodies were selected and added to a new phasor. Lifetime of all the cells was averaged for each slice at each time-point to generate the lifetime time-course.

Electrophysiological recordings in rat spinal neurons

Whole cell clamp recordings were performed in parasagittal slices of lumbar spinal cord from rats as described previously[9,42,43]. For experiments involving PNI rats, all recordings were made from slices ipsilateral to the nerve injury. In BDNF experiments parasagittal spinal cord slices were incubated in BDNF (50 ng/ml) for > 1 h prior to experimentation. For whole-cell experiments involving measurements of E_{GABA} under Cl^- load, borosilicate patch pipettes had a resistance of 4 to 5 MΩ when filled with a potassium methylsulfate-based intrapipette solution[9,43]. Data were filtered during acquisition with a low pass filter set at 2 kHz and sampled at 10 kHz using pClamp 10 (Molecular Devices). Data analysis was performed off-line with Clampfit 10.2 (Molecular Devices). All recordings were performed at physiological temperature (30–34 °C) in standard ACSF[9,42] supplemented with 10 mM 6-cyano-7-nitroquinoxaline-2,3-dione (CNQX), 40 mM D(−)-2-amino-5-phosphonovaleric acid (AP5), and 1 mM TTX. In experiments with BDNF-treated slices, the ACSF was supplemented with 50 ng ml^{-1} BDNF. To study the effects of CLP257 on $GABA_A$ receptor function, a CsCl-based intrapipette solution[42,44] was used and the ACSF was supplemented with the KCC2 inhibitor VU0240551 (10 μM; Tocris Cookson, Ellisville, MO). GABA (1 mM) was puffed approximately 10 μm from the center of the soma for 30 ms. Only neurons with stable access resistance were included for subsequent analysis. Experimental E_{GABA} was extrapolated from the $GABA_A$ I–V relationships.

Nerve injury models and behavioural testing

Under isoflurane anesthesia (induction at 4%, maintenance at 2%) a polyethylene cuff (PNI)[20,28] or loose chromic gut ligatures (CCI)[29] were implanted around the left sciatic nerve of 190–200 g male Sprague-Dawley rats. Mechanical allodynia was quantified by assessing the paw withdrawal threshold using von Frey filaments (Stoelting, USA) using the up and down method[45]. Animals were classified as allodynic when their paw withdrawal thresholds were below 2 g (PNI) or 5 g (CCI) for at least two consecutive days after a constant decrease for > 10 days post-surgery. Allodynia was measured prior to dosing (baseline) on the test day, and then animals received an intraperitoneal dose of vehicle (20% 2-hydroxypropyl-β-cyclodextrin), CLP257 or Gabapentin, or an oral dose of vehicle, CLP290 or Pregabalin. Pregabalin was preferred to Gabapentin for comparison with CLP290 because it has more predictable pharmacokinetics and pharmacodynamics than Gabapentin when given orally.

Evoked field electrophysiological recordings in the superficial dorsal horn

Laminectomies were performed in control and PNI rats (350–450 g) to expose the L4-S1 segments of the spinal cord under isoflurane anaesthesia (induction at 4%, maintenance at 2%). To reduce breathing artefacts the animals were paralyzed with pancuronium bromide (Sigma, USA) and ventilated artificially (SAR-830, CWE, USA). Expired CO2 and body temperature was maintained at 4%. and 37 °C. The rat was placed in a stereotaxic and spinal frame with two clamps fixed on its vertebra to immobilize the spinal cord. A spinal perfusion chamber, continuously perfused with sterile heated (35°C) buffered saline (10 mM HEPES, Sigma-Aldrich, USA), was created by cutting a window in a solidified 4% agar bloc. For drug applications CLP257 was diluted in buffered saline from a DMSO stock

solution to a final concentration of 100 μM (0.1% DMSO) and perfused for 30 min before subsequent measurements were performed to ensure that stable concentrations were reached within the tissue. 4 μM TTX (Sigma/RBI) was used as a control to abolish field responses. A locally designed, automatically controlled, force-feedback mechanical stimulator was used to apply graded and stable mechanical stimulations on the glabrous skin of the paw. Eight or nine graded step pressures covering a large range from non-noxious to noxious stimulation (5–140 g $(mm^2)^{-1}$) were used with a 2 mm^2 tip. A 2–4 min recovery period was allowed between stimuli to minimize sensitization.. In vivo field recording using a glass electrode (1–3 MΩ) were obtained from the superficial section of the dorsal horn (300 μm) that receives input from the glabrous skin of the hind paw. A glass electrode (1–3 MΩ) was mounted on a motorized micromanipulator (Burleigh 6000, USA). The signal was amplified (ER-1 Cygnus Technology, USA), filtered at 0.002–2 KHz, digitized at 20 KHz with a Power1401mkII (CED, UK) and analysed with Spike2 (CED, UK). To evaluate the effect of the mechanical stimulations, we analysed the area under the curve of the field response generated by the different stimuli. Field area was normalized to the maximal control response for each cell and averaged.

Pharmacokinetic analysis

CLP257 and CLP290 (in 20% 2-hydroxypropyl-β-cyclodextrin) were administered IV, IP or PO to adult male Sprague-Dawley rats. Blood samples were collected from the saphenous vein pre-dose, 0.25, 0.5, 1, 2, 4, and 7 h post-dose. Each blood sample (approximately 0.5 ml) was collected into a tube containing an anticoagulant (Na_2-EDTA). Samples were kept on ice until centrifuged. The plasma obtained from each sample was recovered and stored frozen (at −80°C) pending analysis by LC/MS.

Rotorod assay

Baseline motor performance was measured on the day of the test, prior to administration of test compounds, using an accelerating rotorod (IITC). Time on rod was assayed twice for each animal. CLP290 (in 20% 2-hydroxypropyl-β-cyclodextrin), Pregabalin (in 0.9% NaCl) or vehicle (20% 2-hydroxypropyl-β-cyclodextrin) were then administered orally. Rotorod performance was measured again 2 h post-dose. Results are expressed as percent of pre-dose time on rod for each group of animals.

Competitive binding assays

The competitive binding inhibition of 10 μM CLP257 for a number of receptor systems was assessed using validated radioligand competition binding assays under conditions defined by the contractor. Additional information on the assay conditions can be obtained from the contractor's website (www.cerep.fr).

$GABA_A$ receptor automated whole cell patch-clamp

The effect of CLP257 on $GABA_A$ receptor function was assessed using validated automated patch-clamp assays under conditions defined by the contractor. Additional information on the assay conditions can be obtained from the contractor's website (www.cerep.fr).

Toxicological studies

CLP290 (200, 600 and 2000 mg kg^{-1} day^{-1}) and vehicle (20% Captisol) control were administered twice daily by gavage to Sprague-Dawley rats (5 males and 5 females per dose level) for 7 consecutive days. Mortality checks, clinical signs, food consumption and body weights were observed during treatment. At the end of treatment animals were food-deprived overnight and urine was collected for urinalysis. Terminal blood was collected from the abdominal aorta for clinical pathology evaluations followed by necropsy. Blood collected in EDTA-containing tubes was evaluated for complete blood count. Blood collected in citrate-containing tubes was analyzed for activated partial thromboplastin time, and prothrombin time. Blood collected in tubes containing clotting-activator gel was analyzed for comprehensive metabolic panel, A/G ratio (calculated), cholesterol (total), globulin (calculated), phosphorus (inorganic), triglycerides. Urine was analyzed for bilirubin, blood, color and appearance, glucose, ketones, microscopic analysis, pH, protein, specific gravity, urobilinogen, volume. Adrenals, brain, heart, kidneys, liver, lungs, ovaries, pituitary, prostate, spleen, testes, thymus, thyroid with parathyroids, and uterus were trimmed free of fat and weighed. Paired organs were weighed together and organ weight was normalized to terminal body weight. Brain, heart, kidneys, and liver were embedded in paraffin, sectioned and stained. All in vivo toxicological studies were performed blindly by an independent contract research organization.

hERG inhibition of tail current—The inhibitory effect of CLP257and CLP290 on hERG channel tail current amplitude was assessed using validated automated patch-clamp assays under conditions defined by the contractor. Additional information on the assay conditions can be obtained from the contractor's website (www.cerep.fr).

Cytotoxicity—rat hepatoma derived H4IIE cells were cultured in Eagles Minimum Essential Medium with 10% bovine serum and 10% calf serum (Invitrogen). Flat bottom 96-well plates were seeded with 10,000 cells per well 48 hr prior to dosing. On the third day CLP257 (in 0.5% DMSO; 300 μM CLP257 in 1.5% DMSO) was added to the plates. Caspase-3 activity was determined using a caspase substrate (DEVD) labeled with cleavable 7-Amino-4-methylcoumarin (AMC). Following CLP257 exposure, medium was aspirated and PBS added to each well. Plates were stored at −80°C to lyse cells before analysis. Caspase buffer with fluorescent substrate was added to each well and incubated at room temperature for 1 hr. AMC release was measured in a spectrofluorometer (excitation: 360 nm, emission: 460 nm).

Statistics

All data are given as the mean ± SEM unless otherwise started. As data distribution normality (Gaussian) was not assumed, non-parametric tests were used excepted where indicated. Differences between groups were tested by Mann-Whitney test or by Kruskal-Wallis test with *post hoc* Mann-Whitney or Dunn tests. Paired comparisons were analyzed by Wilcoxon signed ranked test. Repeated measures were analyzed by ANOVA or Friedmann test with *post hoc* Dunnet test or Wilcoxon test. Exponential fittings were compared by F test. Sample sizes are consistent with those reported in similar studies. Differences were considered to be significant at $P < 0.05$.

Supplementary Material

Refer to Web version on PubMed Central for supplementary material.

Acknowledgments

This work was supported by grants from the Canadian Institutes for Health Research (CIHR) and the Krembil Foundation to Y.D.K. A Fellowhip from the Savoy Foundation to M.J.B. and the Fonds de la recherche en santé du Québec Chercheur National Program to Y.D.K. We thank T. Kuner for the generous gift of the Clomeleon plasmid.

References

1. Arion D, Lewis DA. Altered expression of regulators of the cortical chloride transporters NKCC1 and KCC2 in schizophrenia. Arch Gen Psychiatry. 2011; 68:21–31. [PubMed: 20819979]
2. Boulenguez P, et al. Down-regulation of the potassium-chloride cotransporter KCC2 contributes to spasticity after spinal cord injury. Nat Med. 2010; 16:302–307. [PubMed: 20190766]
3. Coull JA, et al. Trans-synaptic shift in anion gradient in spinal lamina I neurons as a mechanism of neuropathic pain. Nature. 2003; 424:938–942. [PubMed: 12931188]
4. Hewitt SA, Wamsteeker JI, Kurz EU, Bains JS. Altered chloride homeostasis removes synaptic inhibitory constraint of the stress axis. Nat Neurosci. 2009; 12:438–443. [PubMed: 19252497]
5. Huberfeld G, et al. Perturbed chloride homeostasis and GABAergic signaling in human temporal lobe epilepsy. J Neurosci. 2007; 27:9866–9873. [PubMed: 17855601]
6. Hyde TM, et al. Expression of GABA signaling molecules KCC2, NKCC1, and GAD1 in cortical development and schizophrenia. J Neurosci. 2011; 31:11088–11095. [PubMed: 21795557]
7. Price TJ, Cervero F, de Koninck Y. Role of cation-chloride-cotransporters (CCC) in pain and hyperalgesia. Curr Top Med Chem. 2005; 5:547–555. [PubMed: 16022677]
8. Tornberg J, Voikar V, Savilahti H, Rauvala H, Airaksinen MS. Behavioural phenotypes of hypomorphic KCC2-deficient mice. Eur J Neurosci. 2005; 21:1327–1337. [PubMed: 15813942]
9. Ferrini F, et al. Morphine hyperalgesia gated through microglia-mediated disruption of neuronal Cl(−) homeostasis. Nat Neurosci. 2013; 16:183–192. [PubMed: 23292683]
10. Doyon N, et al. Efficacy of synaptic inhibition depends on multiple, dynamically interacting mechanisms implicated in chloride homeostasis. PLoS Comput Biol. 2011; 7:e1002149. [PubMed: 21931544]
11. De Koninck Y. Altered chloride homeostasis in neurological disorders: a new target. Curr Opin Pharmacol. 2007; 7:93–99. [PubMed: 17182282]
12. Kahle KT, et al. Roles of the cation-chloride cotransporters in neurological disease. Nat Clin Pract Neurol. 2008; 4:490–503. [PubMed: 18769373]
13. Kuner T, Augustine GJ. A genetically encoded ratiometric indicator for chloride: capturing chloride transients in cultured hippocampal neurons. Neuron. 2000; 27:447–459. [PubMed: 11055428]
14. Garbarini N, Delpire E. The RCC1 domain of protein associated with Myc (PAM) interacts with and regulates KCC2. Cell Physiol Biochem. 2008; 22:31–44. [PubMed: 18769030]
15. Inoue K, Yamada J, Ueno S, Fukuda A. Brain-type creatine kinase activates neuron-specific K+-Cl − co-transporter KCC2. J Neurochem. 2006; 96:598–608. [PubMed: 16336223]
16. Simard CF, et al. Homooligomeric and heterooligomeric associations between K+-Cl− cotransporter isoforms and between K+-Cl− and Na+-K+-Cl− cotransporters. J Biol Chem. 2007; 282:18083–18093. [PubMed: 17462999]
17. Lipinski CA, Lombardo F, Dominy BW, Feeney PJ. Experimental and computational approaches to estimate solubility and permeability in drug discovery and development settings. Adv Drug Deliv Rev. 2001; 46:3–26. [PubMed: 11259830]
18. Hiki K, et al. Cloning, characterization, and chromosomal location of a novel human K+-Cl− cotransporter. J Biol Chem. 1999; 274:10661–10667. [PubMed: 10187864]

19. Delpire E, et al. Small-molecule screen identifies inhibitors of the neuronal K-Cl cotransporter KCC2. Proc Natl Acad Sci USA. 2009; 106:5383–5388. [PubMed: 19279215]
20. Mosconi T, Kruger L. Fixed-diameter polyethylene cuffs applied to the rat sciatic nerve induce a painful neuropathy: ultrastructural morphometric analysis of axonal alterations. Pain. 1996; 64:37–57. [PubMed: 8867246]
21. Rivera C, et al. BDNF-induced TrkB activation down-regulates the K+-Cl− cotransporter KCC2 and impairs neuronal Cl− extrusion. J Cell Biol. 2002; 159:747–752. [PubMed: 12473684]
22. Rivera C, et al. Mechanism of activity-dependent downregulation of the neuron-specific K-Cl cotransporter KCC2. J Neurosci. 2004; 24:4683–4691. [PubMed: 15140939]
23. Coull JA, et al. BDNF from microglia causes the shift in neuronal anion gradient underlying neuropathic pain. Nature. 2005; 438:1017–1021. [PubMed: 16355225]
24. Zhang W, Liu LY, Xu TL. Reduced potassium-chloride co-transporter expression in spinal cord dorsal horn neurons contributes to inflammatory pain hypersensitivity in rats. Neuroscience. 2008; 152:502–510. [PubMed: 18262726]
25. Lu Y, Zheng J, Xiong L, Zimmermann M, Yang J. Spinal cord injury-induced attenuation of GABAergic inhibition in spinal dorsal horn circuits is associated with down-regulation of the chloride transporter KCC2 in rat. J Physiol. 2008; 586:5701–5715. [PubMed: 18845615]
26. Cramer SW, et al. The role of cation-dependent chloride transporters in neuropathic pain following spinal cord injury. Mol Pain. 2008; 4:36. [PubMed: 18799000]
27. Jolivalt CG, Lee CA, Ramos KM, Calcutt NA. Allodynia and hyperalgesia in diabetic rats are mediated by GABA and depletion of spinal potassium-chloride co-transporters. Pain. 2008; 140:48–57. [PubMed: 18755547]
28. Pitcher GM, Ritchie J, Henry JL. Nerve constriction in the rat: model of neuropathic, surgical and central pain. Pain. 1999; 83:37–46. [PubMed: 10506670]
29. Bennett GJ, Xie YK. A peripheral mononeuropathy in rat that produces disorders of pain sensation like those seen in man. Pain. 1988; 33:87–107. [PubMed: 2837713]
30. Gilron I. Gabapentin and pregabalin for chronic neuropathic and early postsurgical pain: current evidence and future directions. Curr Opin Anaesthesiol. 2007; 20:456–472. [PubMed: 17873599]
31. Bos R, et al. Activation of 5-HT2A receptors upregulates the function of the neuronal K-Cl cotransporter KCC2. Proc Natl Acad Sci USA. 2013; 110:348–353. [PubMed: 23248270]
32. Kanaka C, et al. The differential expression patterns of messenger RNAs encoding K-Cl cotransporters (KCC1,2) and Na-K-2Cl cotransporter (NKCC1) in the rat nervous system. Neuroscience. 2001; 104:933–946. [PubMed: 11457581]
33. Yang K, Huang ZW, Huang J, Zhang XJ, Xiao BK. Expression of the neuron-specific potassium chloride cotransporter KCC2 in adult rat cochlear. Neurosci Lett. 2008; 441:205–209. [PubMed: 18577424]
34. Mercado A, Mount DB, Gamba G. Electroneutral cation-chloride cotransporters in the central nervous system. Neurochem Res. 2004; 29:17–25. [PubMed: 14992262]
35. Nightingale S. The neuropathic pain market. Nat Rev Drug Discov. 2012; 11:101–102. [PubMed: 22293560]
36. Vargas-Espinosa ML, Sanmarti-Garcia G, Vazquez-Delgado E, Gay-Escoda C. Antiepileptic drugs for the treatment of neuropathic pain: a systematic review. Med Oral Patol Oral Cir Bucal. 2012; 17:e786–793. [PubMed: 22549682]
37. Dharmshaktu P, Tayal V, Kalra BS. Efficacy of antidepressants as analgesics: a review. J Clin Pharmacol. 2012; 52:6–17. [PubMed: 21415285]
38. Smith HS. Opioids and neuropathic pain. Pain Physician. 2012; 15:ES93–110. [PubMed: 22786465]
39. Hudmon A, et al. A mechanism for Ca2+/calmodulin-dependent protein kinase II clustering at synaptic and nonsynaptic sites based on self-association. J Neurosci. 2005; 25:6971–6983. [PubMed: 16049173]
40. Chorin E, et al. Upregulation of KCC2 activity by zinc-mediated neurotransmission via the mZnR/GPR39 receptor. J Neurosci. 2011; 31:12916–12926. [PubMed: 21900570]

41. Digman MA, Caiolfa VR, Zamai M, Gratton E. The phasor approach to fluorescence lifetime imaging analysis. Biophys J. 2008; 94:L14–16. [PubMed: 17981902]

42. Bonin RP, et al. Pharmacological enhancement of delta-subunit-containing GABA(A) receptors that generate a tonic inhibitory conductance in spinal neurons attenuates acute nociception in mice. Pain. 2011; 152:1317–1326. [PubMed: 21396779]

43. Cordero-Erausquin M, Coull JA, Boudreau D, Rolland M, De Koninck Y. Differential maturation of GABA action and anion reversal potential in spinal lamina I neurons: impact of chloride extrusion capacity. J Neurosci. 2005; 25:9613–9623. [PubMed: 16237166]

44. Labrakakis C, Lorenzo LE, Bories C, Ribeiro-da-Silva A, De Koninck Y. Inhibitory coupling between inhibitory interneurons in the spinal cord dorsal horn. Mol Pain. 2009; 5:24. [PubMed: 19432997]

45. Chaplan SR, Bach FW, Pogrel JW, Chung JM, Yaksh TL. Quantitative assessment of tactile allodynia in the rat paw. J Neurosci Methods. 1994; 53:55–63. [PubMed: 7990513]

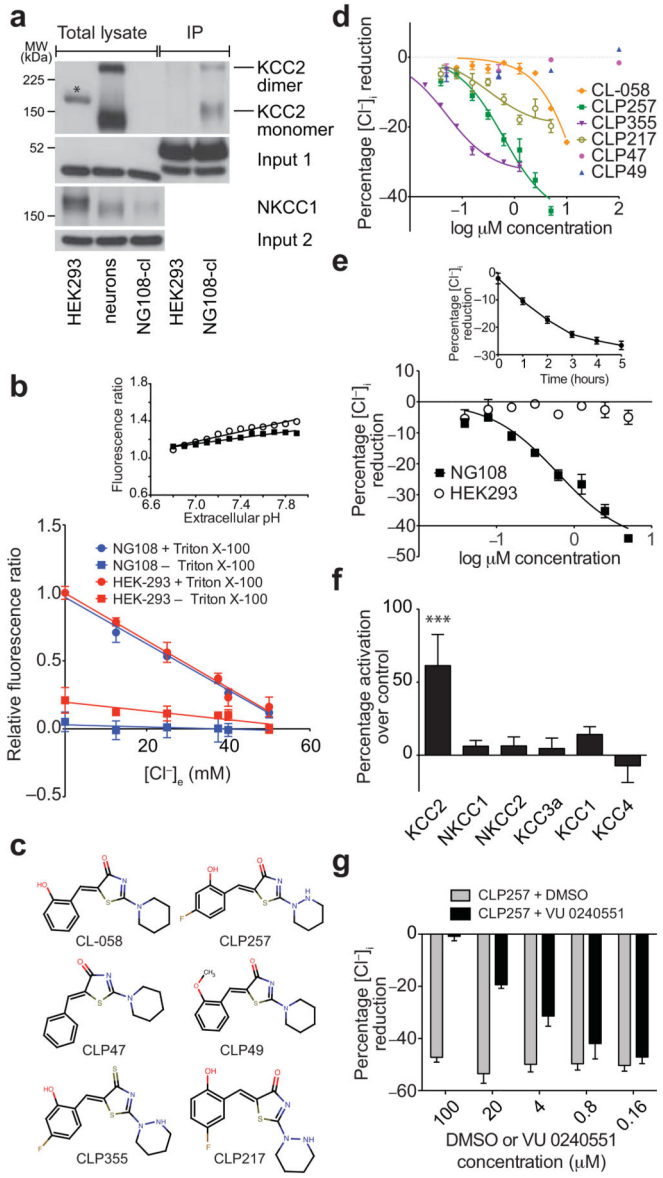

Figure 1. Screening for, and improvement of KCC2-dependent intracellular Cl^- lowering compounds

a) Expression of KCC2 in clomeleon-stably-transfected NG108 (NG108-cl) cells. Immunoblots of KCC2 in HEK293-cl cells (negative control), hippocampal neurons (positive control) and NG108-cl cells (total lysates *vs.* after KCC2 immunoprecipitation; IP). *, non-specific band not observed after IP. Immunoblot of NKCC1 in total lysates of all cell types. Input 1 and 2: β-actin used as loading control. The upper band in Input 1 corresponds to IgGs serving as control for the amount of antibodies used for IP. **b)** Relationship between $[Cl^-]$ and YFP/CFP clomeleon fluorescence ratio. $[Cl^-]_i$ was clamped to $[Cl^-]_e$ by membrane permeabilisation using 0.15% Triton X-100 (means ± SD; n =4 assays). Inset effect of pH on fluorescence ratio (open circles: with 0.15% Triton X-100, closed squares: without Triton X-100; means ± SD; n = 4 assays). **c)** Chemical structures of CL-058 analogues tested in **d). d)** Concentration-response curves of CL-058 hit compound and

selected analogs. **e)** Concentration-response curves of CLP257 in NG108-cl and HEK293-cl (means ± SEM; n = 4 assays). In **c)** and **d)** $[Cl^-]_i$ was measured after a 5 h exposure to compounds. Inset shows $[Cl^-]_i$ response of NG108-cl cells to 1.25 μM CLP257 over time (means ± SEM; n = 4 assays). **f)** Effect of CLP257 pre-treatment on 45 min Rb^+ influx assays in CCCs-expressing *X. laevis* oocytes (means ± SEM; 12 ≤ n ≤20 oocytes. *H*: 41; ***$P < 0.001$). **g)** Effect of the KCC2 antagonist VU0240551 on response to CLP257. Shown are $[Cl^-]_i$ in NG108-cl cells after 5 h exposure to CLP257 500 nM + DMSO vehicle or VU0240551 (means ± SEM; n = 4 assays).

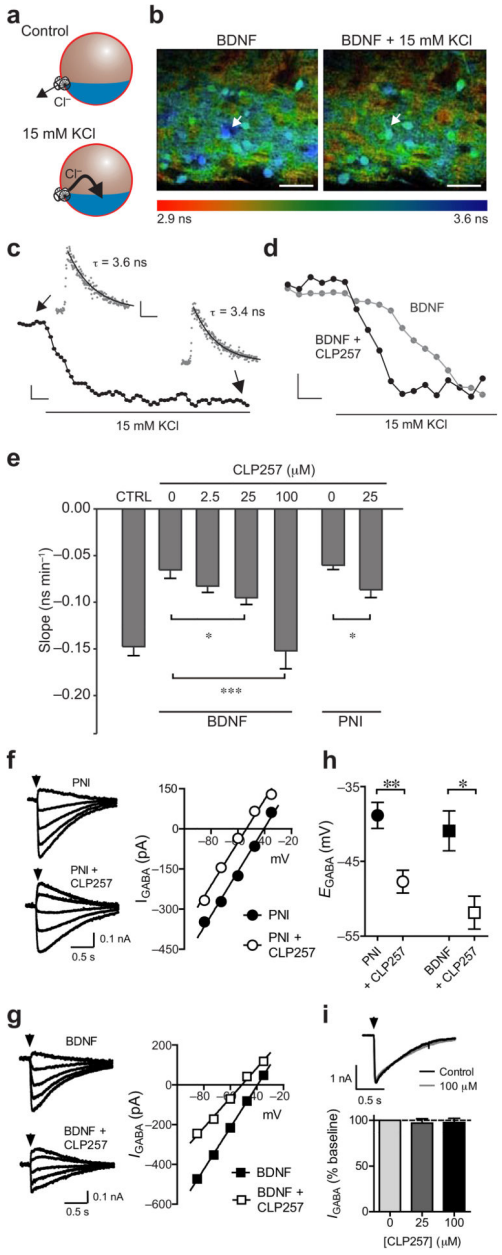

Figure 2. CLP257 restores Cl^- transport in adult spinal cord slices with impaired KCC2 function

a) Diagram illustrating inversion of KCC2 transport upon raising $[K^+]_e$. **b)** Color-coded lifetime image of lamina II cells loaded with the Cl^- indicator MQAE in slices treated with BNDF vs. BDNF with 15 mM $[K^+]_e$; lower lifetime values correspond to high $[Cl^-]$. Scale bar 50 μm. **c)** Time-lapse recording of Cl^- accumulation in the cell bodies of neurons upon extracellular application of 15mM KCl. Measurements taken every 10 s. Scale bars: vertical 50 ps; horizontal 20 s. *Insets*: examples of photon distribution histograms fitted to extract lifetimes shown in **b** (arrow), during the control period (top) and after Cl^- equilibration in 15 mM KCl (bottom). Scale bars: vertical 40 photons; horizontal 20 ns. **d)** Effects of CLP257 on the efficacy of Cl^- transport in lamina II cells. Slope of the change in fluorescence 2 h

after addition of CLP257 (100 μM) to a slice pretreated with BDNF for 2 h (means ± SEM). **e)** Comparison of the rate of Cl^- changes measured in superficial dorsal horn (SDH) neurons in spinal cord slices treated with BDNF or taken from PNI rats, before and 2h after addition of CLP257 ($4 < n < 12$, H: 32; $^*P < 0.05$; $^{***}P < 0.001$). **f–g)** Effect of CLP257 (25 μM, > 1 h) on E_{GABA} in SDH neurons in slices from rats after PNI or BDNF treatment. *Left panels:* responses to 30-ms GABA puffs (black arrowhead) in lamina II neurons in the presence of a Cl^- load (30 mM in the recording pipette*). Right panels: I–V* relationships from representative cells. **h)** Pooled E_{GABA} of neurons from PNI rats under control conditions (n = 11 cells) and treated with CLP257 (n = 8 cells; U: 9, $^{**}P < 0.01$), and from BDNF-treated slices with (n = 8 cells) and without CLP257 (n = 7 cells; U: 7, $^*P < 0.05$). **i)** Quantification of $GABA_A$ responses (normalized to baseline) in neurons after 5 min of CLP257 incubation (25 μM, n = 7 cells, W: −4, $P > 0.05$; 100 μM, n = 5 cells, W: −5, $P > 0.05$) using 120 mM CsCl-filled pipettes and in the presence of the KCC2 antagonist VU0240551. *Inset*: representative responses of SDH neurons to GABA puffs before and after application of CLP257 (100 μM).

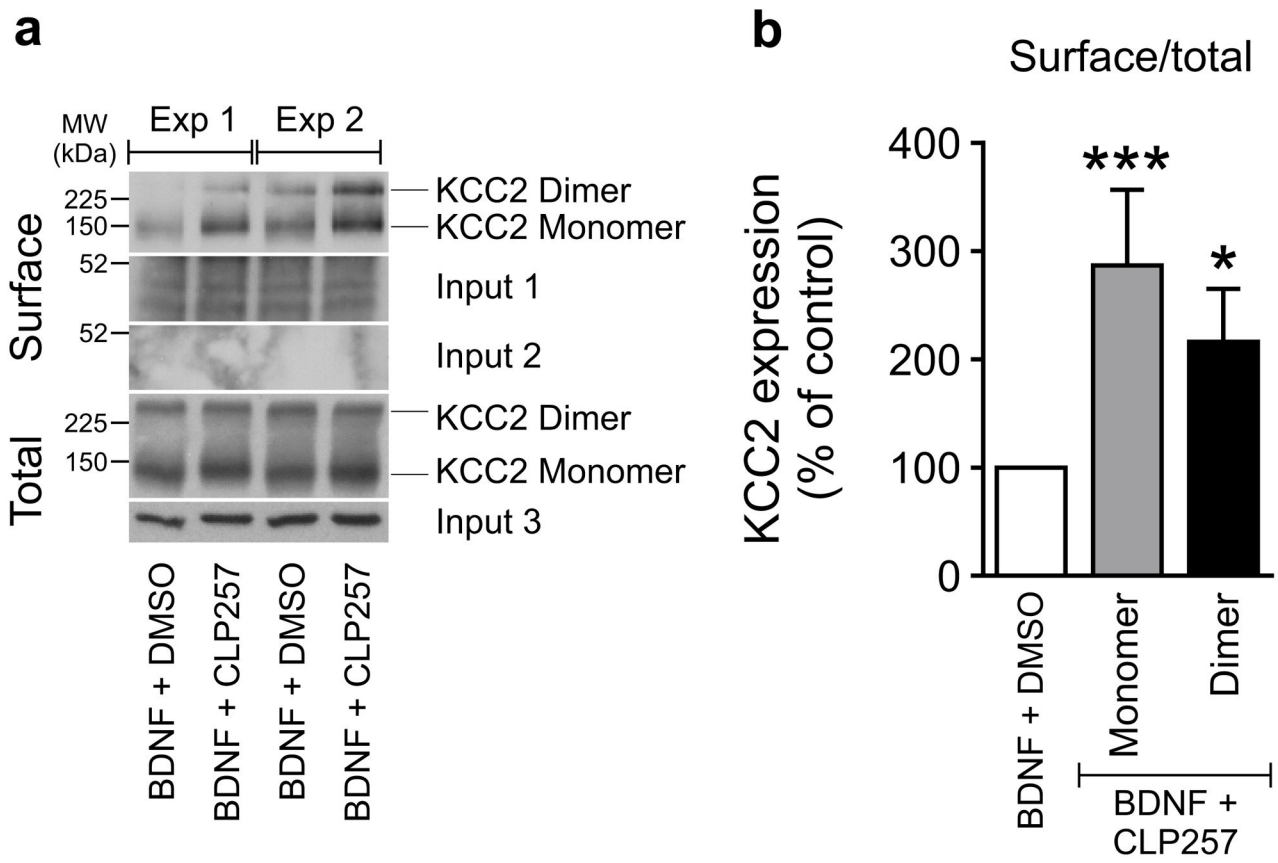

Figure 3. CLP257 increases plasmalemmal KCC2 protein in BDNF-treated adult spinal cord slices

a) Two cell surface biotinylation and total immunoblots (Exp 1 and Exp 2) of KCC2 monomers and dimers following BDNF + 100 μM CLP257 treatment. Input 1: total biotinylated cell surface proteins used as loading control. Input 2: over-exposed film of a β-actin immunoblot showing no signal. Input 3: total β-actin protein used as loading control. **b)** Quantification of the ratio of surface to total KCC2 monomer and dimer expression in response to treatment of slices with BDNF + 100 μM CLP257 *vs.* control BDNF + DMSO; each spinal cord served as its own control (means ± SEM; n = 16 pairs from 16 rats; $W_{monomers}$: 9; W_{dimers}: 26; *$P < 0.05$; ***$P < 0.001$).

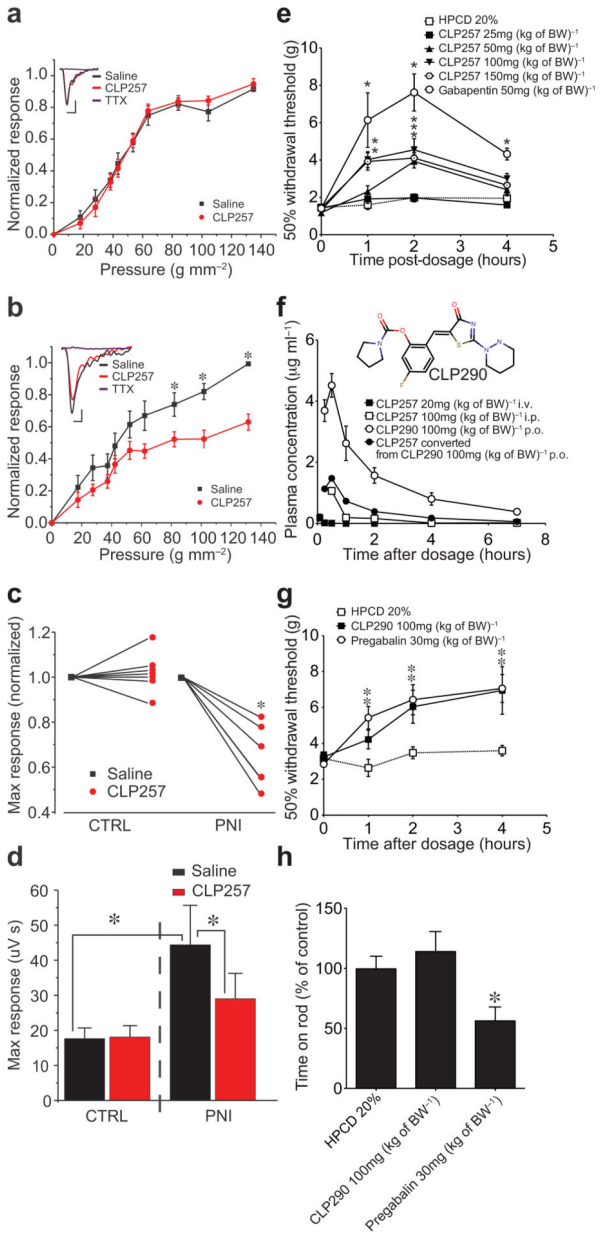

Figure 4. In vivo assessment of the efficacy and pharmacokinetics of CLP257 and its pro-drug CLP290

a) Input/output relationship between the field electrophysiological response recorded in the superficial layers of the spinal dorsal horn and the strength of mechanical stimuli applied to the receptive field (footpad) after local spinal administration of vehicle (saline) or CLP257 in normal animals. *Inset*: Representative example of field responses upon local spinal administration of saline, CLP257 or TTX. (means ± SEM, n = 7 rats). **b)** same graph as in **a)** but in PNI rats (means ± SEM; *W*: 21, $*P < 0.05$). **c)** Effect of CLP257 on the normalized maximal field response in control animals (CTRL, n = 7 rats) and animals with peripheral nerve injury (PNI, n = 6 rats, *W*: 28, $*P < 0.05$). **d)** *Black bars*: Mean (± SEM) maximal field responses to mechanical stimulation of the receptive field in control (CTRL, n = 7 rats)

and PNI rats (PNI, n = 6 rats, *U*: 4, **P* < 0.05). *Red bars*: Effect of CLP 257 application in control (n = 7 rats) and PNI rats (n = 6 rats, *W*: 27, **P* < 0.05). **e)** Effect of CLP257 on paw withdrawal threshold in PNI rats. CLP257 was dissolved in 20% 2-hydroxypropyl-β-cyclodextrin and administered IP (means ± SEM; 8 ≤ n ≤ 10; **P* < 0.05, ***P* < 0.01; *** *P* < 0.001). **f)** Pharmacokinetic profile of CLP257 and the carbamate prodrug CLP290 in rats after IV, IP or PO administration (means ± SEM; n =3 animals per time point). *Inset*: structure of CLP290. **g)** Analgesic effect of CLP290 administered PO in a PNI rat (means ± SEM; 7 ≤ n ≤ 32; **P* < 0.05). **h)** Effect of CLP290 and Pregabalin (at equipotent analgesic dose) on motor performance in rats as measured by time spent on an accelerating rotorod (means ± SEM; 4 ≤ n ≤ 12; *U*: 6; **P* < 0.05). CLP290 was dissolved in 20% 2-hydroxypropyl-β-cyclodextrin.